Solvation Oscillations and Excited-State Dynamics of 2-Amino- and 2-Hydroxy-7-nitrofluorene and Its 2′-deoxyriboside

Venugopal Karunakaran,[†,§] Matthias Pfaffe,[†] Ilya Ioffe,[‡] Tamara Senyushkina,[†] Sergey A. Kovalenko,[†] Rainer Mahrwald,[†] Vadim Fartzdinov,[†] Heinz Sklenar,[£] and Nikolaus P. Ernsting*[,†]

Department of Chemistry, Humboldt University of Berlin, Germany, Department of Chemistry, Moscow State University, Russia, and Max-Delbrück Centre for Molecular Medicine, Berlin, Germany

Received: December 31, 2007; In Final Form: February 18, 2008

Push−pull substituted fluorenes are considered for use as dynamic solvation probes in polynucleotides. Their fluorescence band is predicted (by simulations) to show weak spectral oscillations on the subpicosecond time scale depending on the nucleotide sequence. The oscillations reflect the local far-infrared spectrum of the environment around the probe molecule. A connection is provided by the continuum theory of polar solvation which, however, neglects molecular aspects. We examine the latter using acetonitrile solution as a test case. A collective librational solvent mode at 100 cm^{-1} is observed with 2-amino-7-nitrofluorene, 2-dimethylamino-7-nitrofluorene, 2-hydroxy-7-nitrofluorene, and its 2′-deoxyriboside. Different strengths of the oscillation indicate that rotational friction of nearby acetonitrile molecules depends on the solute structure or that H bonding is involved in launching the librational coherence. Polar solvation in methanol is used for comparison. With hydroxynitrofluorenes, the observation window is limited by intersystem crossing for which rates are reported. A prominent excited-state absorption band of nitrofluorenes at 430 nm can be used to monitor polar solvation. Structural and electronic relaxation pathways are discussed with the help of quantum chemical calculations.

1. Introduction

The solvation of a molecular dipole, created by femtosecond laser excitation, is widely used to study the dynamics of the environment[1−5] such as supercritical fluids,[6−9] micelles,[2,5,10,11] lipids,[12−15] proteins,[16−20] and polynucleotides.[3,21,22] Many fluorescent probes are available for polar solvation dynamics. A fundamental point concerns the "molecularity of solvation",[23] the degree to which the structure of the entire assembly, probe and environment, must be known or controlled for meaningful results. For example, consider solvation in liquids such as acetonitrile, methanol, or water at room temperature. When the distance exceeds several probe diameters, the fluctuating solvent structure can be averaged and replaced, in effect, by a smooth polarizable continuum with dielectric dispersion $\epsilon(\omega)$. The resulting continuum theory of polar solvation[23−26] contains a cavity radius r around the solute as the only structure parameter (see Figure 1). Because the outer spheres contribute significantly, it may be possible for some probes[27,28] to accommodate the remaining molecularity by adjusting r. Another example is provided by the solvation of a well-known[29] coumarin probe which has been linked into polynucleotide (DNA) double helices.[30,31] In this case the dynamics is essentially nonexponential, longer time constants (10−300 ps) coming from the interaction with water molecules and counterions in the hydration layer.[22] Only the relative position of the chromophore in a strand and the length of the duplex seem to matter for the slow dynamics. In both cases, the precise molecular structure is not needed.

Here we consider molecular probes for fast oscillatory dynamics in polynucleotides, which sets different priorities. To observe the relevant time range (50 fs−2 ps), a long fluorescence lifetime is not necessary. However, like in IR spectroscopy, we need the structure of the chromophore linked to 2′-deoxyribose and stacked between nucleobases to analyze the dynamics. The design of a solvatochromic probe must therefore start from structural considerations. Fluorescent 2-amino purine (2AP) is an obvious candidate[3,32,33,34] since it pairs perfectly with thymine;[35] however, a small Stokes shift (690 cm^{-1})[36] and near-UV emission (peaking at 26900 cm^{-1}) preclude its use for technical reasons at present. Instead, we propose 2-amino- and 2-hydroxy-7-nitrofluorene (ANF and HNF, Scheme 1) in DNA as dynamic solvation probes for the femtosecond time scale. ANF was the first compound for which solvent oscillations were shown.[28] Its dynamic Stokes shift exceeds 2000 cm^{-1} even in 1,4-dioxane; therefore, relatively small excursions may still be observed in practice. Also, the fluorene moiety is rigid so that intramolecular wavepackets can be avoided by excitation at or below the peak of the absorption band, and it fits into double-stranded DNA in place of a base pair (see below).

The principle of measurement is illustrated in Figure 1. The dye is optimized so that optical excitation $S_1 \leftarrow S_0$ is accompanied by intramolecular charge transfer, which creates a strong dipole in the excited state. Then, nearby groups begin to align their dipoles with the new electric field around the solute, lowering the energy of S_1 and raising that of S_0 correspondingly. The fluorescence band therefore shifts to lower energies as

* To whom correspondence should be addressed. E-mail: nernst@chemie.hu-berlin.de.
[†] Humboldt University of Berlin.
[‡] Moscow State University.
[£] Max-Delbrück Centre for Molecular Medicine.
[§] Present address: Department of Physics, Northeastern University, 111 Dana Research Center, 110 Forsyth Street, Boston, Massachusetts 02115.

10.1021/jp712176m CCC: $40.75
Published on Web 04/03/2008

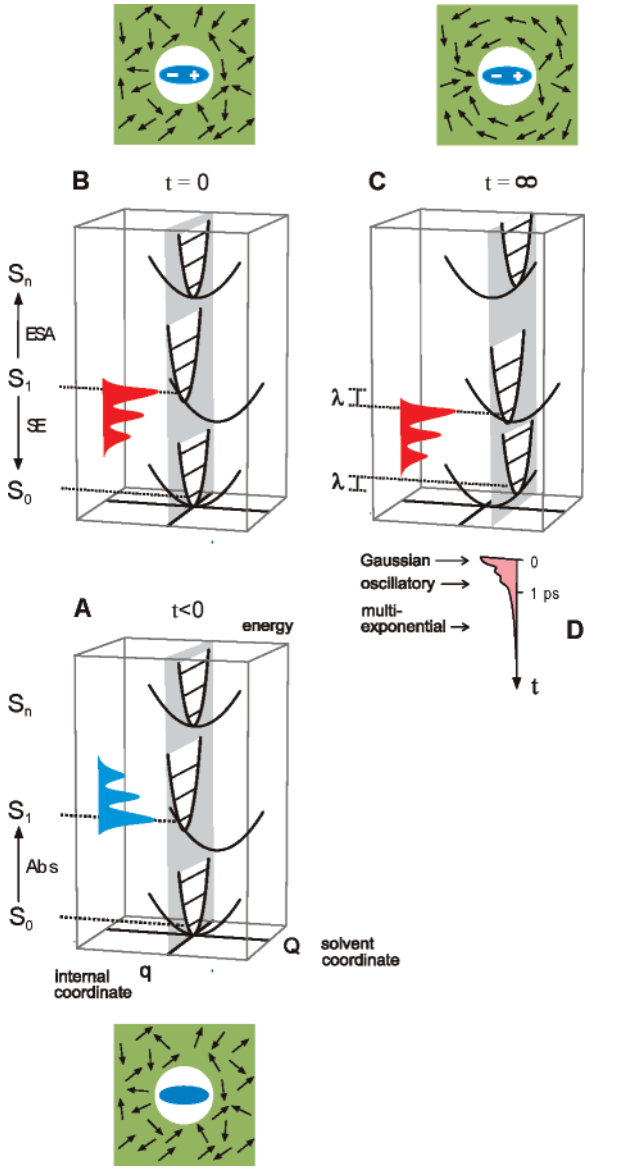

Figure 1. Polar solvation dynamics. A nonpolar probe in the electronic ground state (A) is equilibrated with surrounding dipoles. Femtosecond laser excitation creates a polar excited state (B), but the configuration of the environment is still unchanged. At $t = 0$, the fluorescence or stimulated emission (SE) band overlaps with the $S_1 \leftarrow S_0$ absorption band at the electronic origin. Relaxation along solvent coordinate Q lowers S_1 and raises S_0 by the reorganization energy λ of the environment (C). The time-resolved Stokes shift 2λ of the emission band mirrors the complex dynamics of $Q(t)$ (D).

SCHEME 1

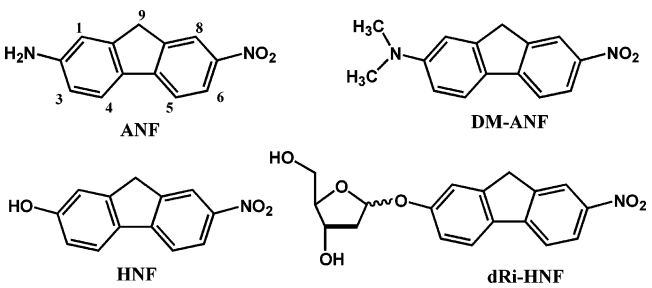

solvation proceeds. After sufficient time (symbolized by ∞), a new equilibrium is reached for the S_1 state (C).

The time-resolved dynamic Stokes shift is defined by $\nu(t) - \nu(\infty)$, where $\nu(t)$ and $\nu(\infty)$ denote the observed emission frequency (for example, band average or peak) at time t and at equilibrium. Normalization provides an experimental relaxation function[37]

$$S(t) = \frac{\nu(t) - \nu(\infty)}{\nu(0) - \nu(\infty)} \quad (1)$$

which reflects the relaxation of the solvent coordinate (Figure 1D). The initial behavior at $t = 0$ is determined by inertial motion of the supramolecular surrounding and is therefore Gaussian,[38,39] in agreement with molecular dynamics simulations[23] and verified by experiment.[28,40−43] The time interval until ~2 ps may, in principle, exhibit weak oscillations that indicate a polarization wavepacket in the environment. Vibrational wavepackets are ubiquitous when *intra*molecular motion is excited in the molecular chromophore itself. However, *inter*-molecular coherence, that is, correlated motion of several solvent molecules,[44−46] should be rare because it is damped by collisions; consequently, only a few reports give experimental evidence of induced solvent oscillations.[28,47,48] Finally, the time scale from about 2 ps until tens of ns is characterized by diffusive motion in a wider macromolecular volume around the probe molecule. Most of the experimental work has been devoted to the time range where the relaxation function is described by multiexponential decay.[21,49−54]

In this paper we test ANF, DM-ANF, HNF, and the 2′-deoxyriboside dRi-HNF (Scheme 1) for their ability to sense and report oscillations of a polar environment. Having future experiments with polynucleotides in mind, we work here, instead, with polar liquids. The bulk of the paper is devoted to an investigation into the photophysical factors that affect the time-resolved fluorescence of the title compounds. In the Experimental Results section we report transient absorption spectra upon femtosecond optical excitation in acetonitrile and methanol. Acetonitrile serves as model environment because it provides a FIR spectrum in a band around 100 cm^{-1} due to librational motion.[55] The band is sufficiently narrow so that a corresponding oscillation for the time-resolved dynamic Stokes shift $S(t)$ is predicted by simple continuum theory. The Discussion section is organized in subsections, each headed with a question which must be answered to enable the DNA project. The first subsection deals directly with DNA double helices having a fluorene probe instead of a base pair. Monte Carlo simulations are used to assess the extent to which local FIR spectra in DNA may differ depending on sequence. From this, the temporal−spectral resolution is found which can distinguish such differences in dynamic solvation experiments. In contrast, the second subsection concentrates on the fluorene chromophores exclusively. By quantum chemical calculations, we characterize the structural and electronic changes which are induced by optical excitation, especially in regard to twisting of the nitro group. Thereafter the observed spectral evolutions of the nitrofluorenes in acetonitrile and methanol are discussed. We question how $S(t)$ can be extracted and which uncertainties are involved. For practical work with polynucleotides, considerations of chemical stability suggest that 2-hydroxy-7-nitrofluorene (HNF) is incorporated for a first series of experiments. We ask to what extent a rising triplet population interferes with solvation measurements after a few picoseconds. In a final subsection, continuum predictions are compared with observations for the molecular probes, that is, molecularity is examined. There is evidence that acetonitrile librations are damped depending on the structure or that H bonding is involved in launching the librational coherence.

2. Materials and Methods

2.1. Materials. ANF and alkylated derivatives like DM-ANF were synthesized by palladium-catalyzed reductive amination and substitution of halofluorenes.[56] The preparation of HNF was achieved in 4 steps.[57−60] dRi-HNF was synthesized by reacting HNF with 1′α-chloro-3′,5′-di-*O*-toluoyl-2′-deoxy-D-ribose in the presence of activated molecular sieve. Solvents for spectroscopy were of UV grade (Merck UVASOL).

2.2. Monte Carlo Simulations. Conformations of double-stranded polynucleotides were sampled by an all-atom Monte Carlo (MC) technique. It is based on local conformational moves of the sugar−phosphate moiety while all bond lengths are kept constant. The independent variables include the backbone dihedral angles γ ($O_1'-C_5'-C_4'-C_3'$) and ϵ ($C_4'-C_3'-O_3'-P$), the backbone bond angle ($C_3'-O_3'-P$), and the glycosidic angle χ ($O-C_1'-N-C_8$ or $-C_6$). Structural variations are accomplished by a chain-breakage/closure algorithm.[61] The aromatic bases and chromophores are treated as rigid bodies with three translational and three rotational degrees of freedom. The number of altogether 14 independent variables per nucleotide is reduced to 12 by describing the conformation of the furanose ring through its pseudo-rotation amplitude and phase. The Cornell AMBER force field[62] is employed; the MC acceptance criterion follows the Metropolis algorithm and includes Jacobian factors associated with the chain-breakage/closure algorithm and the pseudo-rotation description. The polyanionic DNA is neutralized by sodium counterions which can move translationally. Solvation by water is treated statically by letting the dielectric constant depend on distance r[63]

$$\epsilon(r) = \epsilon_w - (\epsilon_w - 1)[(rS)^2 + rS + 2]\exp(-rS)/2 \quad (2)$$

with parameters $\epsilon_w = 78$ and $S = 0.16$ Å^{-1}. The approximation is justified because computational results[64,65] are in good agreement with experimental data. It should be emphasized that we seek DNA structure fluctuations by the embedded molecular probe; therefore, explicit water is not essential for the simulations. The implicit solvent treatment allowing for rapid equilibration of the counterion cloud, together with the high acceptance of large step sizes for local conformational moves, is the most important feature of our procedure. After 10^6 MC cycles, accumulated averages of properties are converged and become independent of the initial conformation. The latter, including the counterion cloud, was previously generated and energy-minimized by the JUMNA program.[66]

2.3. Electronic Structure Calculations. A first set of quantum chemical calculations was performed for ANF in the ground-state geometry only, for the purpose of including the chromophore in the Monte Carlo simulations. The geometry was calculated (in vacuo) on the DFT B3LYP/6-311G(d,p) level with Gaussian 98;[67] it agrees with the structure from X-ray diffraction[68] (∼0.01 Å standard deviation of bond lengths). Effective atomic charges $q_i(S_0)$ were obtained by fitting the molecular electrostatic potential, which was calculated on the MP2/6-31G(d)//B3LYP/6-311G(d,p) level. To simulate the solvatochromism of the $S_1 \rightarrow S_0$ emission band, one needs the difference charge distribution $q_i(S_1) - q_i(S_0)$ when all nuclear modes in S_1 are fully relaxed. Instead, the difference charge distribution at the optimized ground-state geometry was calculated with TD B3LYP/6-311G(d,p)//B3LYP/6-311G(d,p).[67]

A second set of calculations concentrated on the excited electronic states of ANF and HNF (also in vacuo), depending on the substituents and their conformation. DFT and TDDFT calculations were carried out with the PRIRODA software, employing a fast implementation of the resolution-of-identity technique.[69] The PBE exchange-correlation functional of GGA type[70] and a built-in TZ2P basis set ((11s6p2d/6s3p2d) for second row atoms and (5s1p/3s1p) for hydrogen atoms) were used. Single-point CIS calculations of the spectra of excited states were at the DFT geometries, with the PC GAMESS software[71] and Dunning's cc-pVTZ basis set obtained from the EMSL basis set exchange.[72]

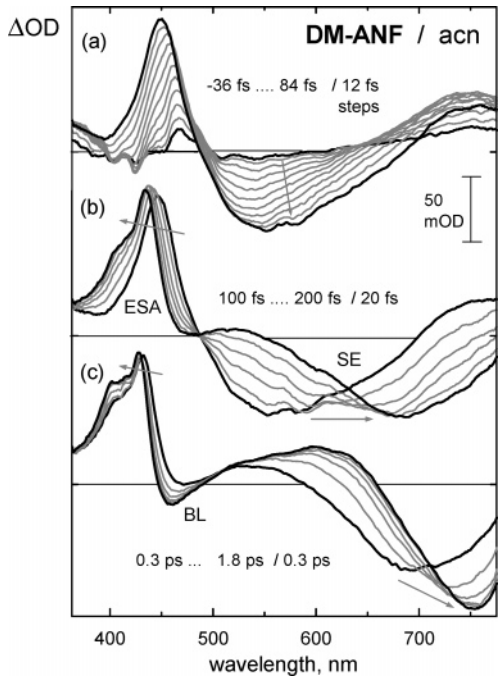

Figure 2. Transient absorption spectra of DM-ANF in acetonitrile upon excitation at 402 nm and with detection polarized at the magic angle. BL, bleach; SE, stimulated emission; ESA, excited-state absorption. The solvent signal has been subtracted. Delay times are given as insets, and arrows show the direction of the evolution. In a, the pump and probe pulses overlap temporally, causing a coherent spectral contribution which includes sharp structure from stimulated Raman scattering (see text).

2.4. Optical Spectroscopy. Transient absorption spectra were measured by pump/supercontinuum−probe spectroscopy[73] with excitation at 402 or 360 nm. The solution ideally had an absorbance of ∼0.5 at the pump wavelength, but because of small internal cell thickness (0.3 mm), lower absorbances had to be used in some cases. Transmitted and reference white-light beams were separately dispersed by imaging spectrographs and registered with photodiode arrays in the range of 360−775 or 275−685 nm (for white light generated at 480 or 402 nm, respectively). The laser repetition frequency was 120 Hz, and the pump beam was chopped at 60 Hz to record pump-induced spectral changes. Fifty individual records were averaged for a given probe delay of a time scan, and results from 3 to 5 scans were averaged. The resulting spectra were then time-corrected for the chirp of the supercontinuum. Baseline noise was better than 5×10^{-4} rms.

Measurements were performed with the pump and probe polarizations parallel, perpendicular, and at the magic angle, both with the sample solution and with the pure solvent. The latter give the pump−probe intensity cross correlation, which can be described by a 65 fs (fwhm) Gaussian shape over the entire probe region. Variations of the pump pulse energy in the range of 0.13−1.0 μJ (150 μm spot diameter) had no effect on the transient spectral shapes. Stationary optical absorption and emission spectra were recorded as in ref 68.

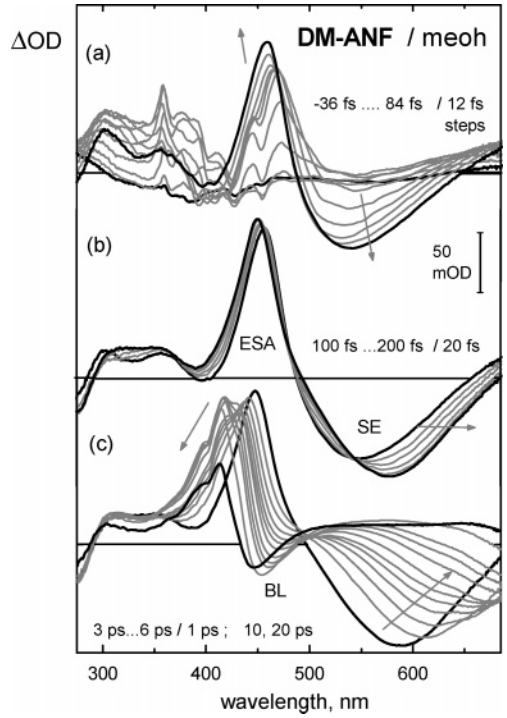

Figure 3. Transient absorption spectra of DM-ANF in methanol from excitation at 402 nm and detected with parallel polarization. The solvent signal has been subtracted.

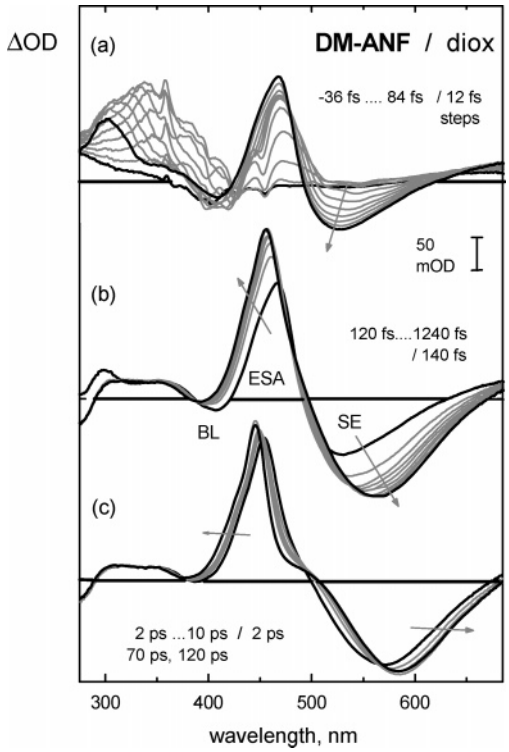

Figure 4. Transient absorption spectra of DM-ANF in dioxane, as in Figure 3.

3. Experimental Results

Figures 2−6 show transient absorption spectra of DM-ANF (which is a solvatochromic absorption standard[74]) in acetonitrile, methanol, and dioxane. Remeasured[28] results for ANF[75] look similar and are not shown. Spectral features and stages are explained for solutions in acetonitrile, Figure 2. The middle panel covers the evolution from 100 fs when the pump pulse is over until 200 fs. Induced optical density $\Delta OD > 0$ corresponds to excited-state absorption (ESA), and $\Delta OD < 0$ indicates stimulated emission (SE) in the fluorescence region of 500−770 nm. Initially the SE band appears close to the ground-state

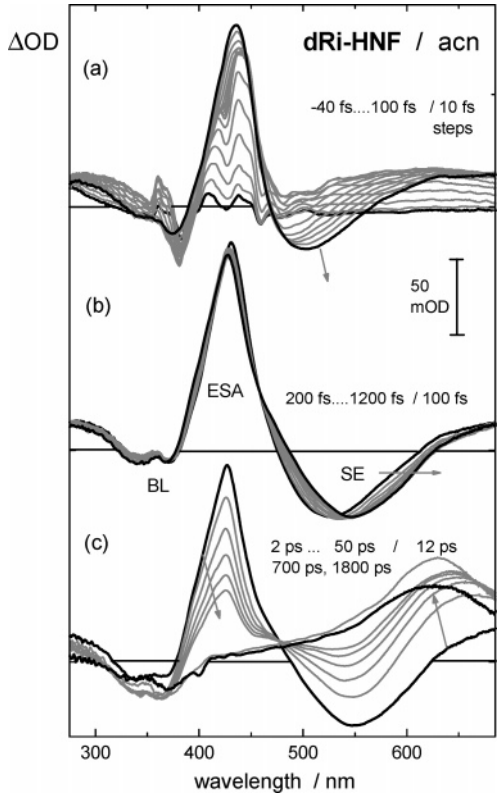

Figure 5. Transient absorption spectra of the 2′-deoxyriboside dRi-HNF in acetonitrile with excitation at 402 nm and detection polarized at the magic angle; the solvent signal has been subtracted. The shift of the red SE flank (horizontal arrow in b) is used to monitor solvent relaxation (Figure 17).

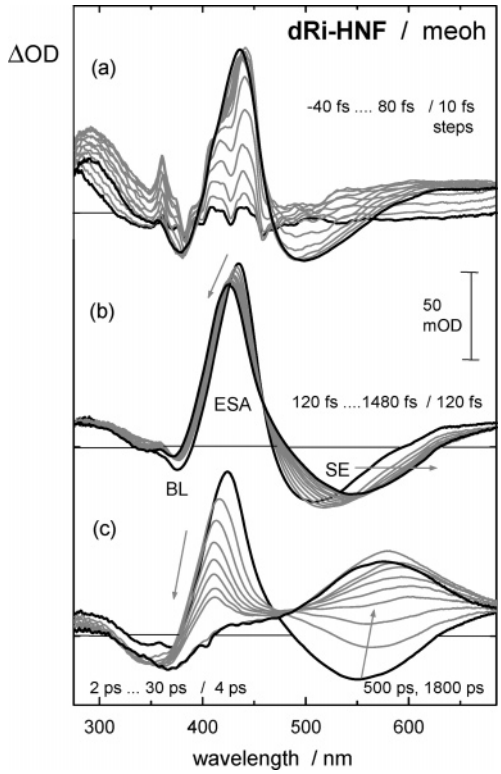

Figure 6. Transient absorption spectra of dRi-HNF in methanol, as in Figure 5.

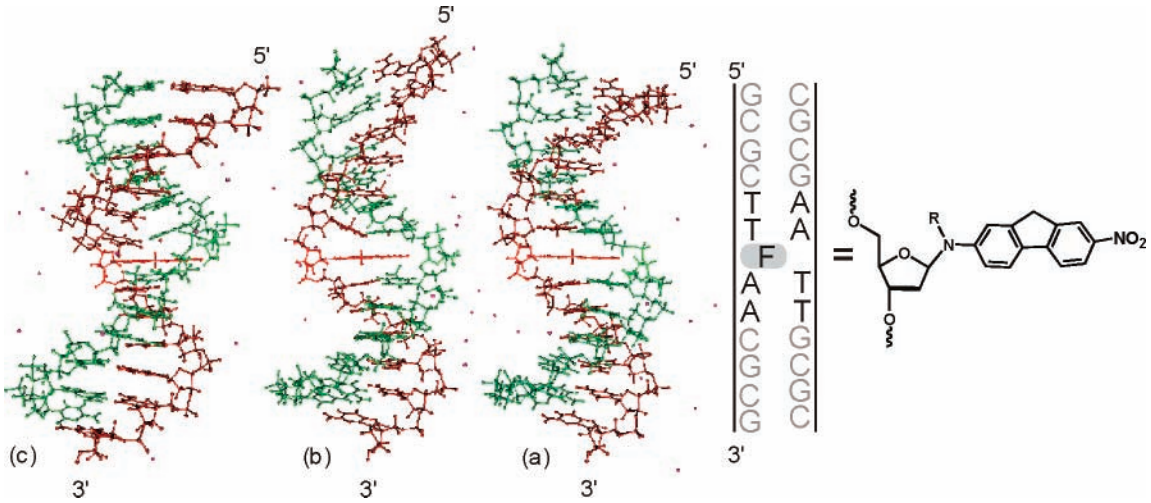

Figure 7. Typical duplex oligonucleotide used in simulations of solvation dynamics. Configurations correspond to the energy minimum (a) or have average energy (b,c).

TABLE 1: Properties of the Singlet Excited States of ANF and HNF, Calculated by TDDFT/CIS in Vacuo[a]

state	oscillator strength	energy of vertical excitation 1000 cm^{-1}	relative stationary point energy 1000 cm^{-1}	stationary point dipole moment, *D*
		ANF		
S_0		0	0	8.8
S_1	0.31	20.4	11.53 (19.2)	26.5 (19.9)
S_2	$<10^{-6}$	26.7	18.9	7.1
energy of S_1-S_2 crossing: 22.6				
		HNF		
S_0		0	0	6.5
S_1	0.31	22.5	15.7 (21.5)	21.5 (17.3)
S_2	$<10^{-6}$	26.8	18.9	4.5
energy of S_1-S_2 crossing: 22.7				

[a] Values in parentheses refer to the local planar minimum; see text.

absorption, and excited-state absorption is observed at around 750 nm. The SE band moves to the red with an observed total shift of 4580 cm^{-1} and overcompensates the red ESA. Simultaneously, the sharp and dominant ESA band (450.5 nm peak at 100 fs) shifts to higher energy by 740 cm^{-1} until 200 fs. The evolution from 0.3 to 1.8 ps is shown in the lower panel. Bleached absorption (BL) appears at around 460 nm because the blue ESA no longer dominates there, and the SE continues its slide to the red until the quasistationary emission frequency is reached at 3 ps. Thereafter, the amplitude decreases on a 50 ps time scale.

The pump−probe process can be described as a third-order perturbation of the material sample by the optical field.[76] Photoexcitation consists of two interactions with the pump field, and the induced polarization is probed by interaction with the supercontinuum field. For panels b and c, the pump pulse is well separated from the probe pulse so that the threefold interaction must have the sequence pump−pump−probe. The ESA, SE, and BL signals are correspondingly termed "sequential"; they are caused by population in the excited state S_1 and by the hole created in the ground state S_0. Instead, the upper panel covers the initial time range when pump and probe pulses overlap temporally. In this case the interaction order may also be mixed, for example, pump−probe−pump. This gives rise to a "coherent" signal which follows the pump/probe intensity cross correlation,[77,78] whereby it may quantified.[79] A coherent spectrum can be understood in terms of SE, ESA, and BL contributions as before, with the addition of stimulated resonant Raman scattering, which is recognized by sharp vibronic structure. The solvent also contributes coherent signal, which is measured separately and subtracted.

Solvation in methanol (Figure 3) is used for reference because low-frequency oscillations are not expected in this case (see below). Similar behavior is observed for 200 fs, albeit with a different extent and dynamics of spectral shifts. The shifts continue on a 10 ps time scale in parallel to amplitude decay of the SE, which therefore never reaches a stationary emission frequency. After 20 ps the emission has disappeared from the observation window entirely, even though the BL and ESA features still amount to about half of their maximal amplitude.

1,4-Dioxane (Figure 4) is of interest because its dielectric constant is similar to what is assumed for the internal DNA region. The upper panel again gives the early spectra, the vibronic structure being due to Raman scattering from the solute chromophore. The next two panels show a small red and blue shift of the SE and ESA bands, respectively. The latter is observed at a longer wavelength compared to that for acetonitrile solution so that the negative BL contribution is overcompensated. A change of peak value for SE(t) is balanced by corresponding changes of the width, leading to nearly constant ΔOD at around 560 nm. Thereafter, the amplitude remains constant, in agreement with the relatively long fluorescence lifetime.[80]

The oxygen-bridged derivative dRi-HNF is stable during DNA synthesis. Figures 5 and 6 show its spectra in acetonitrile and methanol, and equivalent results for the parent HNF are presented in the Supporting Information. The spectral evolution of the hydroxy derivatives is similar to that of the amino analogues, but the similarity lasts only for 3−4 ps. Before, during the period of interest of 100 fs−1.5 ps in the middle panels, the SE band is well defined so that the dynamic Stokes shift may be estimated. The following 10 ps time scale (lower panels) sees the rise of a new band which dominates all other features by ∼500 ps. Independent nanosecond measurements of HNF in acetonitrile identify the new band as triplet−triplet absorption. In methanol, a small difference between dRi-HNF and HNF is recognized, between 100 fs and 1.5 ps, which may be due to different H-bonding abilities of the two compounds.

4. Discussion

4.1. Are Substantial Differences of Local FIR Spectra Likely in DNA? A qualitative preview (Figures 7−9) of

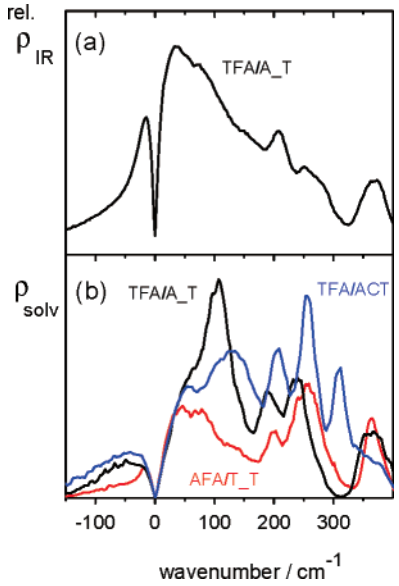

Figure 8. The calculated IR spectrum of a 13mer double helix (a) does not vary with sequence.[82] Polar interaction between the solvation probe and the DNA matrix is described by a "local IR spectrum", which depends strongly on the neighboring nucleobases (b).

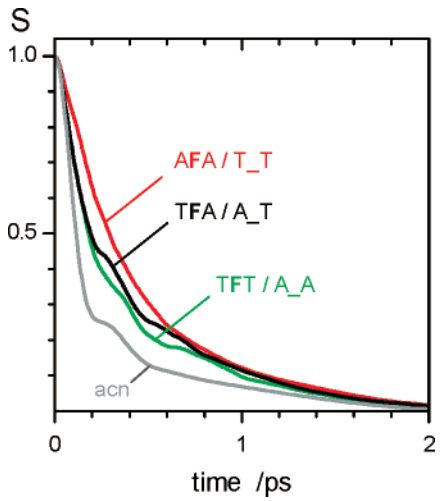

Figure 9. The solvation relaxation of ANF in various DNA sequences is predicted to oscillate weakly. The precision of measurements that is needed to extract the oscillations can be estimated from these curves. Polar solvation in acetonitrile (acn, from the continuum model) is shown for comparison.

dynamic solvation in DNA is afforded by Monte Carlo simulations[81] in combination with "instantaneous normal mode" theory.[39] A typical 13mer duplex oligonucleotide is shown in Figure 7. The nitrofluorene F occupies the central site in one strand, and the opposite site is taken to be abasic for the figure. The aim of the simulations is to see how sensitively the solvation dynamics depends on the neighboring base pairs. After femtosecond excitation, can we expect the fluorescence from F to oscillate spectrally during the first few picoseconds, and how do the oscillations depend on the base sequence? In the simulations, ANF was linked to 2′-deoxyribose by a β-glycosidic bond with the amino nitrogen atom. The resulting aminal is labile but can be protected by an acyl group R (in the simulations R = H). For a given sequence, about 10^6 configurations are generated in a distribution at room temperature. The configuration of minimal energy (Figure 7a) has a helical form which

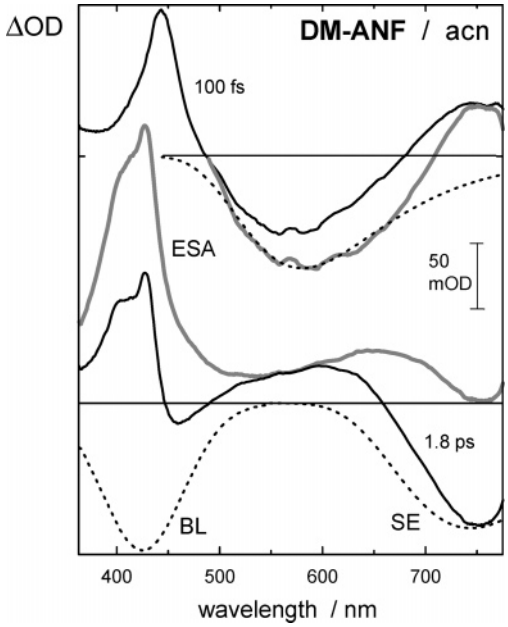

Figure 10. Spectral decomposition for DM-ANF in acetonitrile (Figure 2). Top panel: transient spectrum (black solid line) at 100 fs just after the pump pulse is over; estimate of stimulated emission band (gray, see text); and shifted stationary emission band (dashed). Bottom panel: transient spectrum (black solid line) at 1.8 ps when the spectral shift has ceased; bleach and stationary stimulated emission (dashed); and the resulting excited-state absorption (gray).

corresponds to B-DNA, but at average energy (Figure 7b,c), significant structure fluctuations are seen in the vicinity of the probe moiety. The ability to report such structure fluctuations by the oscillations which they impose on the fluorescence shift $S(t)$ is the primary aim of the probe design. Solvation by surrounding water is instead expected to be diffusive at all times, given our experimental (temporal and spectral) resolution. Its contribution to $S(t)$ will be overdamped and thus obscure the oscillatory structural part. To focus on the latter, surrounding water is simulated as a static dielectric continuum so that water dynamics is excluded.

The FIR spectrum of a duplex oligonucleotide can be obtained by plotting $|\partial\mu_0/\partial x_i|^2$ of instantaneous normal modes x_i against vibrational frequencies ν_i, where μ_0 is the dipole moment of the macromolecule in S_0. After summing over the ensemble, a smooth spectrum is obtained, as for example in Figure 8a. The FIR spectra of different sequences are found to be practically indistinguishable. However, instead of the dipole moment for every configuration, one may calculate a polar interaction energy between the chromophore and its environment

$$\Delta E_{\mathrm{pol}} = \sum \frac{\Delta q_j q_k}{\epsilon(r_{jk}) r_{jk}} \qquad (3)$$

Here the various Δq_j represent changes of atomic charge in the chromophore upon emission $S_1 \rightarrow S_0$. The q_k are the partial atomic charges on all other sites of the supramolecular structure, that is, they are external to the chromophore. Their distances r_{jk} also depend on the normal coordinates, while $\epsilon(r_{ji})$ accounts for dielectric screening (cf. section 2.2). By plotting $|\partial\Delta E_{\mathrm{pol}}/\partial x_i|^2$ and averaging over all configurations, one obtains a spectral density $\rho_{\mathrm{solv}}(\nu)$ of solvation. It reflects the dynamics of the chromophore's dipole change in the internal electric field and may therefore be considered a "local FIR spectrum". Such local spectra are shown in Figure 8b. They are highly structured by

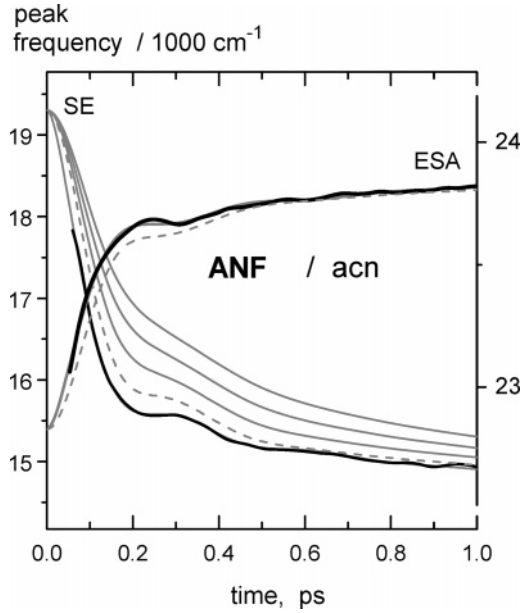

Figure 11. Dynamic frequency shifts (thick solid lines) of the ANF stimulated emission band (SE) in acetonitrile and of the excited-state absorption band (ESA, on a 3× expanded ordinate scale at the right). Dashed lines correspond to polar solvation from simple continuum theory with $n_{cav} = 1.6$. The other gray lines have $n_{cav} = 2.0$, 2.4, and 2.8.

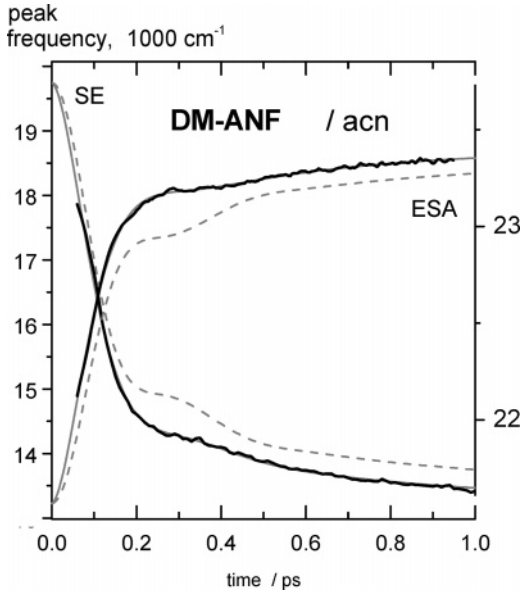

Figure 12. Dynamic frequency shifts of DM-ANF in acetonitrile, as in Figure 11. Polar solvation curves calculated with $n_{cav} = 1.6$ are shown for comparison (dashed lines).

comparison and depend sensitively on the neighboring nucleobases. Solvation curves $S(t)$ may be calculated from $\rho_{solv}(\nu)$,[39,82] and results for various sequences are compared in Figure 9. In order to resolve oscillations for an assumed Stokes shift of 2000 cm^{-1}, the position of the evolving emission band must be determined at every instant to ± 30 cm^{-1}.

4.2. Is Nitro Twisting in the Excited State an Important Interfering Process? Let us return to the nitrofluorene compounds themselves. The electronic ground state and the lowest excited states were calculated by density functional theory (DFT and time-dependent TDDFT, respectively) for ANF and HNF. The frontier orbitals HOMO-1 (n), HOMO (π), and LUMO (π^*) are not visibly affected when the donor substituent is varied.[80] The $S_1(\pi^*) \leftarrow S_0(\pi)$ transition involves charge transfer from the donor-substituted to the nitro-substituted benzene moiety, whereas the $S_2(\pi^*) \leftarrow S_0(n)$ transition is essentially localized on the nitro group. The nature of the S_1 and S_2 states and their relative energies are confirmed by CIS calculations free of self-interaction error. Table 1 provides some properties of singlet excited states for the two chromophores. Relative energy values require a systematic shift for comparison with the experimental data, and polar states will be more stabilized in the liquid phase.

Geometry relaxation from the Franck−Condon-excited S_1 state generally proceeds via rotation (twisting) of the nitro group accompanied by pyramidalization. In the global S_1 minimum, the O−N−O and fluorene planes have become perpendicular. Intersection with S_0 is predicted (by TDDFT) to be close so that internal conversion should be the main deactivation channel. However, a metastable planar S_1 conformation is created by a small barrier along the twisting coordinate, allowing for transient stabilization of the excited population. This planar conformation is characterized by minor (below 0.03 Å) alterations of the bond lengths with respect to the S_0 geometry that are distributed over the whole molecule. The observed stimulated emission is attributed to this region of the S_1 potential energy surface. The absence of intramolecular wavepackets after $S_1 \leftarrow S_0$ excitation (subsection 4.5 below) is consistent with the calculated geometry change; the high-frequency modes which are displaced, such as C−C or N−O bond stretches, cannot be coherently excited by our 40 fs pump pulses, while the few active low-frequency modes are accessible to external forces and appear to be overdamped. Data for the planar conformation are indicated by parentheses in Table 1.

The dark state S_2 is similar to S_0 in having a planar geometry but with a considerably shortened (by 0.13 Å) C−NO_2 bond and somewhat elongated (0.06 Å) N−O bonds. Its potential energy minimum lies below that of the planar S_1 conformation (cf. Table 1). Here one meets the first quantitative difference between HNF and ANF. In the latter molecule, S_2 is negligibly favored over planar S_1 which, however, should be stabilized preferentially by solvation. We conclude that S_2 is not involved in the transient evolution of ANF or DM-ANF following optical excitation. In HNF, on the other hand, the S_2 minimum lies under planar S_1 with a more pronounced energy gap, and an S_1/S_2 intersection is located relatively low. This point will be taken up when intersystem crossing is discussed (subsection 4.4).

The higher-lying singlet states of HNF and ANF have their stationary points above the $S_1 \leftarrow S_0$ vertical excitation energy and are therefore not relevant for the evolution of S_1. Of more interest are the lowest triplet states. When the nitro group is in-plane, the energy gap between the two lowest triplet states T_1 and T_2 is calculated to be insignificant. Upon twisting, the gap increases considerably. This behavior derives from the fact that the β-HOMO and β-LUMO of T_1 (which exchange their roles in T_2) become linear combinations of the HOMO and HOMO-1 of S_0 whereas the α-HOMO remains similar to the LUMO of S_0. The holes in the β set are thus "averaged" in comparison to S_1 and S_2. As a consequence, the stationary point of T_1 (2.17 eV above that of S_0 in ANF and 2.26 eV above that in HNF) is characterized by a moderately twisted, nonpyramidalized geometry.

4.3. How Can Dynamic Solvation of the Excited State be Quantified from Transient Absorption Spectra? The decomposition of transient absorption spectra is explained with DM-ANF in acetonitrile as before (Figure 2). The components BL, SE, and ESA were already discussed; now we try to characterize the SE band for every delay time t quantitatively. The spectrum at 100 fs just after the pump pulse is over and at 1.8 ps when the evolution has ceased (∞) are reproduced in Figure 10. In

between, spectral oscillation of the BL part would indicate vibrational coherence of chromophores remaining in the ground state, but this is not observed. The BL component may therefore be considered constant on the time scale of the measurement; it is proportional to the spectrum $\sigma_{BL}(\nu)$ of the stationary absorption cross section. At $t = \infty$ (lower panel) the SE band is similarly provided by the stationary emission cross section $\sigma_{SE} \propto fqd(\nu)/\nu^2$ where fqd is the fluorescence quantum distribution.[83] The amplitudes of the two components are related because the transition dipole moment for the $S_1 \leftarrow S_0$ and $S_1 \rightarrow S_0$ bands should be identical[84]

$$\int_{band} \sigma_{BL}(\nu)/\nu d\nu = \int_{band} \sigma_{SE}(\nu)/\nu d\nu \qquad (4)$$

However, a common scale factor must still be determined. This is done by subtracting BL and SE from the transient absorption at late time so that a stationary ESA spectrum remains. The scaling factor is varied so that ESA ≥ 0 for all probe frequencies ν, and the resulting spectral components are also shown in the lower panel. Band shapes $\sigma(\nu)/\nu$ are generally fitted by one or several log-normal functions,[85] and parameters for stationary absorption and emission of aminonitrofluorenes in many solvents are given in ref 68.

The evolution from 100 fs to $t = \infty$ is examined next. For this purpose, the ESA(∞) spectrum found previously is assumed to apply also for $t < \infty$, in which case subtraction of BL + ESA(∞) from the transient spectrum would give the corresponding SE(t). The result for $t = 100$ fs is shown as a gray wide line in the upper panel of Figure 10. The inferred emission band is not <0 everywhere, implying that the ESA spectrum is not exactly constant across the emission region, but a large section resembles the stationary emission band quite well. The latter is therefore shifted to a higher peak frequency $\nu(t)$ where the width and amplitude are optimized (dashed line) to match the peak region of the inferred stimulated emission spectrum. The transition dipole moment is kept constant during this adjustment. The SE$-\nu$(t) curves for ANF and DM-ANF in acetonitrile are shown in Figures 11 and 12, and results for methanol solutions are provided as Supporting Information.

One may ask what can be known about the evolution of weaker ESA bands which are hidden under the broad evolving SE band. For an answer, we turn the argument around and assume that the SE evolves from its time-zero shape to the final form[68] strictly according to polar solvation. The $S(t)$ curve calculated with the continuum model (Figure 9) is used to shift the peak position in acetonitrile

$$\nu(t) = [\nu(0) - \nu(\infty)]\cdot S(t) + \nu(\infty) \qquad (5)$$

whereas the width Δ and asymmetry γ change faster

$$\Delta = [\Delta(0) - \Delta(\infty)]\cdot[1 - \sqrt{1 - S^2(t)}] + \Delta(\infty) \qquad (6)$$

(and analogous for γ) as prescribed for Brownian oscillators.[86] Then BL + SE(t) (their amplitudes coupled by eq 4) are subtracted from every transient spectrum to yield the corresponding ESA(t). A common scaling factor is found as before. Selected decompositions of this kind in Figure 13 provide the following view of $S_n \leftarrow S_1$ absorption in the emission range. A well-defined band B settles into position ($\lambda_{max} \approx 660$ nm) by 150 fs. The remaining change suggests a weaker broad band C which originally appears at the red observation edge (775 nm) and moves to the blue with solvation, to emerge between A and B at late time. The dynamic blue shift of C is estimated to be ~5000 cm^{-1}, equivalent to the red shift of the SE band. C

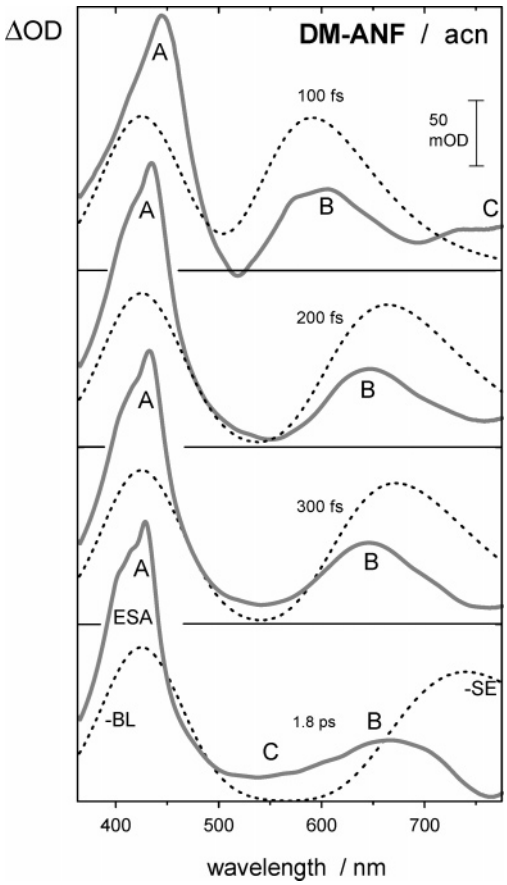

Figure 13. Alternative spectral decomposition for DM-ANF in acetonitrile (Figure 2; BL and SE bands are inverted compared to those in Figure 10). The SE band shape is assumed to follow polar solvation according to the continuum model (see text). This allows an assessment of weaker ESA bands B and C underneath.

would therefore show a transition $S_n \leftarrow S_1$ to an excited state S_n which has roughly the same dipole moment as S_0. Now it is instructive to view the transient spectra in Figure 2 again directly; the apparent increase of stimulated emission[87] between 0.3 and 1.8 ps (panel c) is explained as moving off of the stationary ESA band B. Note however that neither decomposition is unique, and corresponding conclusions are speculative.

The prominent ESA band, which shifts from 450.5 (100 fs) to 428.6 nm (peak at $t = \infty$) in acetonitrile, was already shown to reflect solvation dynamics.[28] Note that the dynamic shift of 1130 cm^{-1} is almost twice the fluorescence Stokes shift that 2-amino purine undergoes in water.[36] The peak frequency of the strong ESA band is also entered in Figures 11 and 12. It presents an alternative observable for the solvation state which may be used when the emission window is too narrow (DM-ANF/MEOH) or obscured by incipient triplet absorption (HNF). The spectral relaxation curves will be discussed together below.

4.4. Which Observation Limits are Imposed by Intersystem Crossing in Hydroxynitrofluorenes? The rise of triplet absorption complicates the observation of the stimulated emission band with hydroxynitrofluorenes. The decomposition of transient absorption spectra into bands for optical transitions becomes inconclusive, and other methods are needed to characterize the dynamic Stokes shift of emission. Before, however, it is useful to examine the intersystem crossing process separately, for example, of dRi-HNF/acn as seen in Figure 5c. By analyzing the spectral evolution through principle components, we find time constants $\tau_1 = 8.3$ ps and $\tau_2 = 51.4$ ps. In Figure 14, the late evolution is represented as a kinetic

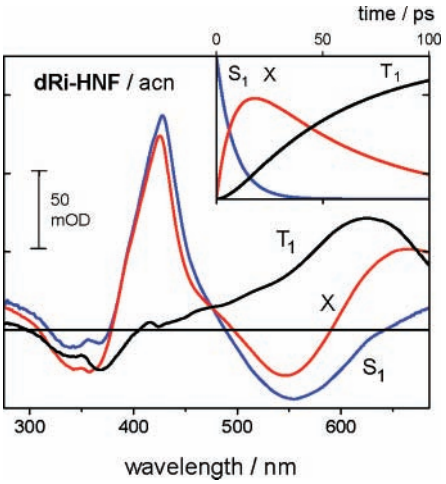

Figure 14. Picosecond transient absorption ($t \geq 6$ ps) of dRi-HNF in acetonitrile is modeled as a kinetic sequence $S_1 \rightarrow X \rightarrow T_1$, with polar solvation complete before S_1 is reached. Shown are results from principal component analysis. The triplet absorption spectrum was identified on the 20−400 ns time scale. X is a virtual state describing the spectral evolution and may not have physical meaning.

TABLE 2: Rate Constants $S_1 \xrightarrow{k1} X \xrightarrow{k2} T_1$ for Intersystem Crossing in Hydroxynitrofluorenes[a]

	solvent	k_1/ps^{-1}	k_2/ps^{-1}
dRi−HNF	acn	0.12 ± 0.03	0.019 ± 0.003
	MEOH		0.090 ± 0.003
HNF	acn	0.11 ± 0.03	0.024 ± 0.003
	MEOH		0.123 ± 0.003
	diox		0.081 ± 0.007

[a] Error margins are given for 99% confidence.

sequence[88] $S_1 \xrightarrow{k1} X \xrightarrow{k2} T_1$. The triplet absorption spectrum was measured independently from 20 to 400 ns and found to be identical to the final spectrum here. Note that the T_1 state does not absorb around 420 nm where S_1 has the prominent ESA band. In methanol the triplet rise is faster and only an effective change $(S_1,X) \xrightarrow{k2} T_1$ can be identified. The evolution of HNF in 1,4-dioxane[80] is seen to be dominated by fast intersystem crossing. Rate constants are collected in Table 2.

Returning to dRi-HNF in acetonitrile (Figure 14), what could the reaction $S_1 \rightarrow X$ be that takes place on a 10 ps time scale? Polar solvation is ruled out since its slowest mode has rate constant $\Lambda_{so} = 1.56$ ps^{-1} (Table 2). Nitro rotation is a possibility which is supported by our quantum chemical calculations for HNF. As the nitro group twists away from the fluorene plane, the dark S_2 state could be admixed through vibronic coupling. The emission strength would be reduced and the acquired nπ^* character would enable intersystem crossing. Both effects are observed for X. It is also conceivable that X represents a biradicaloid intermediate.

Fast solvation by acetonitrile was already noted for dRi-HNF in Figure 5b. Another view is provided by time traces ΔOD-(λ_i,t), where probe wavelengths λ_i are chosen on the blue and red flank of the SE band − an approach which will be explored next. The flanks of the SE band are defined by ΔOD halfway between the ESA maximum in the red and the SE minimum, which are assumed to bracket the amplitude of the band at a given time. The corresponding traces are shown in Figure 15. The interval around $t = 0$ contains coherent and sequential contributions as described earlier. From about 100 fs only the sequential contribution remains, which, in this spectral region,

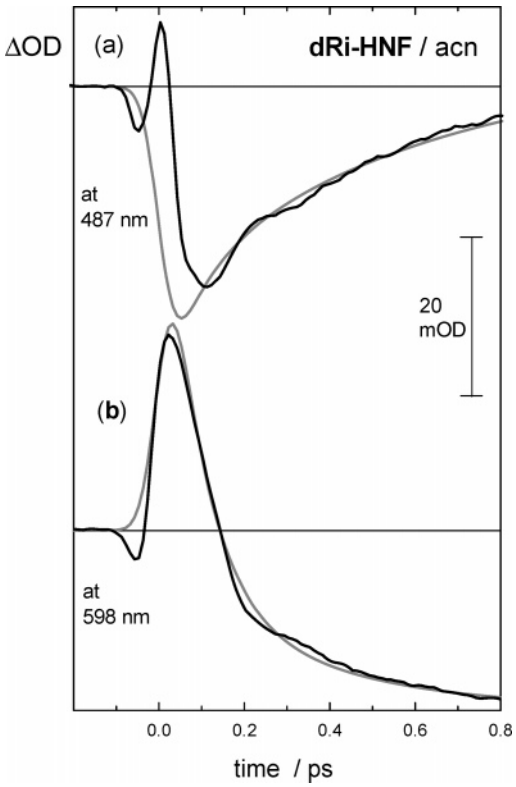

Figure 15. Solvent oscillation of acetonitrile surrounding dRi-HNF, seen by absorption traces (black lines) at the blue and red flanks of the SE band (cf. Figure 5). Traces from a multiexponential fit of the sequential spectral evolution are shown for reference (gray lines).

derives from SE and ESA transitions only. The dynamic red shift is seen by a decrease of the (negative) stimulated emission signal at the blue flank (a) and simultaneous increase at the red (b). Note a weak shoulder in both traces at ∼340 fs, with opposite sign indicating that the SE band is displaced slightly to the blue from the main motion at this moment.

Principal component analysis was also applied to the spectral evolution of dRi-HNF/acn for 5 ps. A Gaussian $G(t)$ and derivatives $G'(t)$ and $G''(t)$ were used to define the coherent contribution,[79] and three (G-convoluted) exponential time functions were sufficient to describe the sequential contribution. In this way the coherence can be removed from early transient spectra, and the best multiexponential description of the evolution is obtained. For example in Figure 15, gray lines show the coherence-free time traces ΔOD(λ_i,t) which result for the two probe wavelengths. A frequency modulation of the emission band until ∼0.5 ps is recognized by comparison with the measured traces. We also find that the coherent signal at around $t = 0$ is large at 487 nm and relatively small at 598 nm. This difference is seen better in Figure 16 where the component spectra at time zero are shown (thick black and gray lines, the sequential part at $t = 0$ scaled by 2 as if the full pump fluence had acted). The induced spectrum at 260 fs is given for comparison. The blue flank of the SE band is found to be covered by strong coherence and the prominent ESA band is close, rendering quantitative analysis uncertain there. The red flank, on the other hand, is not overlaid by coherence, and excited-state absorption seems to be spectrally flat at early time, so that an observable for spectral shift and oscillation can be defined here.

The relative position $\nu(t)$ of the emission band is therefore measured by the wavenumber of the half-point on the red flank (as described above). The dynamic Stokes shift of dRi-HNF/

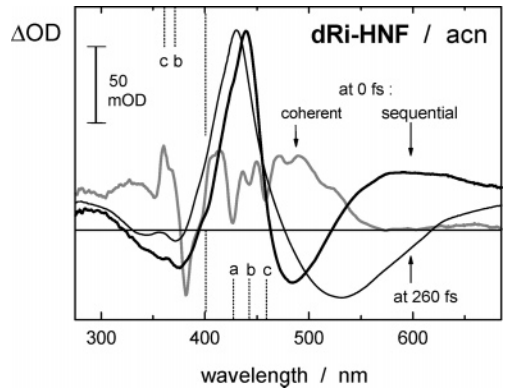

Figure 16. Coherent and sequential spectra at time zero from a global multiexponetial fit for dRi-HNF in acetonitrile (Figure 5). The transient spectrum at 260 fs is given for comparison. Dashed vertical lines mark the pump wavelength and stimulated Raman bands ((a) 1250, (b) 2200, (c) 3000 cm^{-1}); arrows indicate the probe wavelengths in Figure 15.

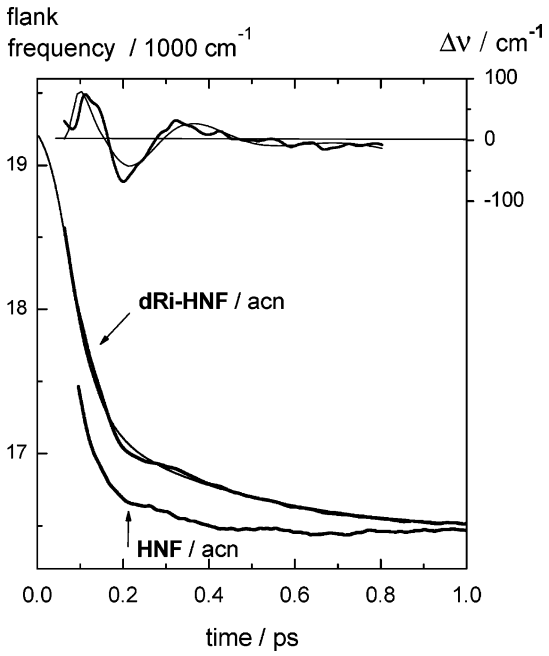

Figure 17. Dynamic shift of the stimulated emission band of dRi-HNF and HNF in acetonitrile (black lines) from monitoring of the red flank. A hump at 0.34 ps indicates a librational wavepacket (100 cm^{-1}) in the solvent. The gray line results from fitting the spectral evolution with exponential functions. Deviations from it are shown in the inset for the measured flank position (thick solid line) and for polar solvation by acetonitrile (thin, see text).

acn is shown in Figure 17 (black line) superimposed on the corresponding curve from factor analysis (thin gray). The damped spectral oscillation of the emission band is noted by comparison, and the difference of the two curves is enlarged in the inset. The oscillation is absent when measurements of dRi-HNF in methanol are analyzed in the same manner (Figure 18).

4.5. To What Extent Does the Observed Solvation Dynamics Depend on the Fluorene Probe? The spectral relaxation of excited ANF and HNF chromophores in polar environments is now compared and discussed. For this purpose, time-dependent band positions $\nu(t)$ must be translated into the corresponding relaxation function $S(t)$, which requires knowledge of the initial position $\nu(0)$ (eq 1). However, observations at around $t = 0$ are generally obscured, either by solvent Raman[89] signal in the case of fluorescence measurements or

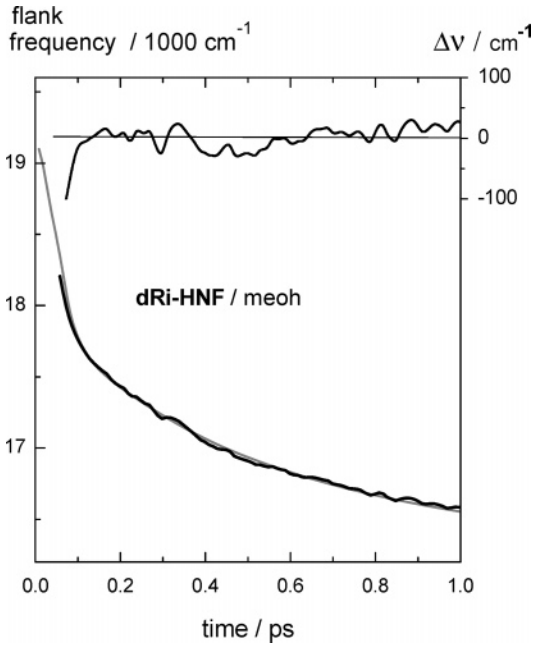

Figure 18. Dynamic Stokes shift of dRi-HNF in methanol, as in Figure 17, for comparison.

by the coherent signal when transient absorption is monitored. Instead, the accessible data points $\nu(t)$ must be fitted with eq 5 where $\nu(0)$ is one of the fit parameters. The choice of form for $S(t)$ is crucial for meaningful results and must be discussed first. One may compare with the relaxation of coumarin probes, which have been examined most intensely by transient fluorescence[29] as well as transient absorption,[90] but never have acetonitrile solvent oscillations been observed with them (this will be discussed below). As a reference for solvent-induced oscillations, we must therefore resort to molecular dynamics simulations[44−46] or to continuum theory.[27] Here, we calculate the time-dependent solvation of a dipole from the dielectric dispersion $\epsilon(\omega)$ of the bulk liquid. First, $\epsilon(\omega)$ is expressed by optical line shapes of Brownian oscillators with angular frequency ω and damping constant γ (results are given in the Supporting Information). The probe molecule then enters the calculation through a refractive index n_{cav} of the cavity that it occupies.[27] In this way, a theoretical relaxation curve is obtained which accurately reflects the dielectric properties of the solvent from the microwave through the far-infrared up to and including the infrared region. Finally, the result is convoluted with our temporal apparatus function, a Gaussian of 65 fs fwhm, which is equivalent to observing $\epsilon(\omega)$ up to 510 cm^{-1}. It turns out that the various curves for acetonitrile that are generated when n_{cav} is increased from 1 (empty cavity) may be expanded into Brownian oscillators in the time domain. Their relaxation functions are

$$S_{ud}(t) = \exp(-\gamma t/2)\left[\cos \omega_1 t + \frac{\gamma}{2\omega_1} \sin \omega_1 t\right]$$

$$S_{cd}(t) = \exp(-\gamma t/2)\left[1 + \frac{\gamma}{2} t\right]$$

$$S_{od}(t) = \exp(-\gamma t/2)\left[\cosh \Omega_1 t + \frac{\gamma}{2\Omega_1} \sinh \Omega_1 t\right]$$

$$S_{so}(t) = \exp(-\Lambda t) \quad (7)$$

for the cases $\omega_1 = \sqrt{\omega^2 - \gamma^2/4} > 0$ (underdamped), $\omega^2 = \gamma^2/4$

TABLE 3: Parameters Describing the Spectral Shifts of Nitrofluorenes in Acetonitrile (eqs 5, 7, and 8)[a]

		(fig)	a_{ud}	ω_{ud} /ps^{-1}	γ_{ud} /ps^{-1}	a_{cd}	ω_{cd} /ps^{-1}	Λ_{so} /ps^{-1}	$\nu(0)$ /cm^{-1}	$\nu(\infty)$ /cm^{-1}	st $\nu(0)$ /cm^{-1}
polar solv.	$n_{cav} = 1.6$	(11)	0.20	18.8 ± 0.3	11.9 ± 1.6	0.51	13.6	1.56	na	na	
ANF	SE peak	(11)	0.12	20.2 ± 0.4	10.2 ± 2.4	0.62	20.5	*1.56*	19305 ± 150	*14640*[b]	21040
ANF	ESA peak	(11)	*0.12*	*20.2*	*10.2*	*0.62*	*20.5*	*1.56*	22830	23877	
DM-ANF	SE peak	(12)	0.38	*18.8*	20.5 ± 2.6	0.35	*13.6*	*2.37*	19750 ± 130	13308	19580
DM-ANF	ESA peak	(12)	0.68	*18.8*	27.2	0.04	*13.6*	*2.37*	21570	23400	
dRi-HNF	SE flank	(17)	0.22	18.5 ± 0.7	17.2 ± 7	0.42	13.3	0.49	*19200*[c]	15670	

[a] Values in italics were transferred from more significant measurements and not varied in the fit; st: from stationary spectra.[94] Errors (for 99% confidence on the basis of the pertinent fit) are given for selected parameters only. $\sum a_i = 1$. [b] From steady-state fluorescence. [c] From multiexponential extrapolation.

TABLE 4: Parameters Describing the Spectral Shifts of Nitrofluorenes in Methanol (eqs 5 and 9)

		(fig)	a_G	ω_G /ps^{-1}	a_1	τ_1 /ps^{-1}	a_2	τ_2 /ps^{-1}	τ_3 /ps^{-1}	$\nu(0)$ /cm^{-1}	$\nu(\infty)$ /cm^{-1}	st $\nu(0)$ /cm^{-1}
polar solv.	$n_{cav} = 1.6$	(S5)	0.20	14.1 ± 0.2	0.35	0.43 ± 0.01	0.15	3.6 ± 0.3	12.0	na	na	
ANF	SE peak	(S5)	0.24	*14.1*	0.34	0.65 ± 0.12	0.42	3.1 ± 0.2	*a*	20180 ± 500	*13150*[b]	21190
ANF	ESA peak	(S5)	0.20	*14.1*	0.40	*0.65*	0.21	*3.1*	*12.0*	22323 ± 30	*24530*[c]	
DM-ANF	SE peak[d]	(S6)	0.27	10.8	0.03	*0.65*	0.61	*3.1*	*12.0*	19246	*12500*	19860
DM-ANF	ESA peak	(S6)	0.15	*14.1*	0.31	*0.65*	*0.40*	*3.1*	*12.0*	21479 ± 30	*24330*[c]	
dRi-HNF	SE flank	(18)	0.42	20.5 ± 0.3	0.58	0.568 ± 0.005	*a*	*a*	*a*	*19100*[e]	*16270*[c]	

[a] $a_i = 0$. [b] From steady-state fluorescence. [c] Final reading. [d] Observation limited to 0.1−2.5 ps. [e] From multiexponential extrapolation; otherwise as that in Table 2.

(critically damped), $\Omega_1 = \sqrt{\gamma^2/4 - \omega^2} > 0$ (overdamped), and $\Lambda = \omega^2/\gamma$ if $\omega \ll \gamma/2$ (strongly overdamped). Normalized relaxation curves for solvation in acetonitrile are generally written as

$$S_{acn}(t) = a_{ud}S_{ud}(\omega_{ud},\gamma_{ud},t) + a_{cd}S_{cd}(\omega_{cd},t) + a_{so}S_{so}(\Lambda_{so}) \quad (8)$$

with $a_{ud} + a_{cd} + a_{so} = 1$. The FIR bands of methanol are broad, and oscillations of the spectral shifts are neither seen nor expected. In this case the solvation function is written[29] as

$$S_{MEOH}(t) = a_G\exp\{-\omega_G^2 t^2/2\tau_G^2\} + a_1\exp\{-t/\tau_1\} + a_2\exp\{-t/\tau_2\} + a_3\exp\{-t/\tau_3\} \quad (9)$$

The determination of optimal parameters is described next. For a start, the acetonitrile solvation curve from continuum theory is calculated with $n_{cav} = 1.6$ (it is seen later that this comes closest to the dynamics observed with ANF). The parameters in eqs 7 and 8, which describe this curve, are given in Table 3, first row. Librational motion of acetonitrile is captured by the term having $\omega_{ud} = 18.8$ ps^{-1} and $\gamma_{ud} = 11.9$ ps^{-1}, corresponding to the FIR absorption band which peaks at 100 cm^{-1}. With this estimate for $S_{acn}(t)$, the measured data $\nu(t)$ for a given solute (ANF, DMANF, or dRi-HNF) in acetonitrile and for a given observable (ESA peak, SE peak, or SE flank) can be extrapolated with the help of eq 5 to estimate $\nu(0)$. Thereafter, most parameters are allowed to vary in a nonlinear least-squares fit, and the results are also collected in Table 3. Optimal values for ω_{ud} and γ_{ud} are reasonably independent and significant, but solutions for Λ_{so}, $a_{cd,so}$, and $\nu(\infty)$ (if unknown) tend to be correlated and are therefore not meaningful by themselves. For methanol solutions, the same procedure is followed using $S_{MEOH}(t)$ (eq 9); results are collected in Table 4. Simulated curves $\nu(t)$ are always shown in the pertinent figures.

The relaxation functions of the nitrofluorenes in acetonitrile are shown in Figure 19. The dipole relaxation in a dielectric continuum ($n_{cav} = 1.6$, black line) and the normalized Stokes shift of fluorescence from Coumarin 153[29] (gray) are given for comparison. The most important observation is that all nitrofluorenes exhibit an oscillatory feature at ≈340 fs. Its solvent origin is established by the similarity with the calculated relaxation curve and by the absence in methanol. The shoulder at ≈340 fs is thus identified as a recurrence of the vibrational mode which underlies the acetonitrile FIR band at 100 cm^{-1}. This band has been assigned to librational motion.[55] It follows that the nitrofluorene probes detect a librational wavepacket in the acetonitrile solvent shell which is launched by suddenly altering the probe's charge distribution through optical excitation (Figure 20).

The strength of the librational recurrence is reflected in the damping constant γ_{ud}. Although error margins are large, a trend may be discerned: agreement with polar solvation for ANF but larger damping for the substituted compounds DM-ANF and dRi-HNF. We can think of three explanations for this effect. (i) As the structure of the probe is enlarged, the spatial correlation between nearby solvent molecules is perturbed and effectively lowered. Two adjacent acetonitrile molecules in a solvation shell sample an increasingly wider range of the interaction between them, compared to their counterparts in the bulk liquid. An acetonitrile molecule in a solvation shell is therefore subjected to additional stochastic torques, at the cost of correlated torques, as the solute structure is extended. The damping constant for librational motion is thus increased. (ii) An alternative possibility (also illustrated in Figure 20) is that H bonding in ANF enhances the solvent libration. First, note that acetonitrile can accept H bonds; its Kamlet−Taft acidity and basicity parameters[91,92] are $\{\alpha,\beta\} = \{0.19, 0.31\}$, which may be compared with {0, 0.76} for DMSO and {1.17, 0.18} for water. Upon excitation, the $CH_3-C\equiv N\cdots H_2N-$ hydrogen bonds are strengthened, causing an additional torque on the H-bonded solvent molecules (*a* and *c* in the figure) and kick-starting the solvent libration (*d*).[93] An indication for this mechanism is provided by the initial frequency $\nu(0)$ which was found by extrapolating the earliest data points back to $t = 0$. For an example, consider the peak of the stimulated band of DM-ANF/acn (Table 3, fourth row). The extrapolated $\nu(0)$ comes close to the "time-zero" value (last column) from a comparison of stationary absorption and fluorescence data.[94] That method involves 2-methylbutane as the reference solvent,

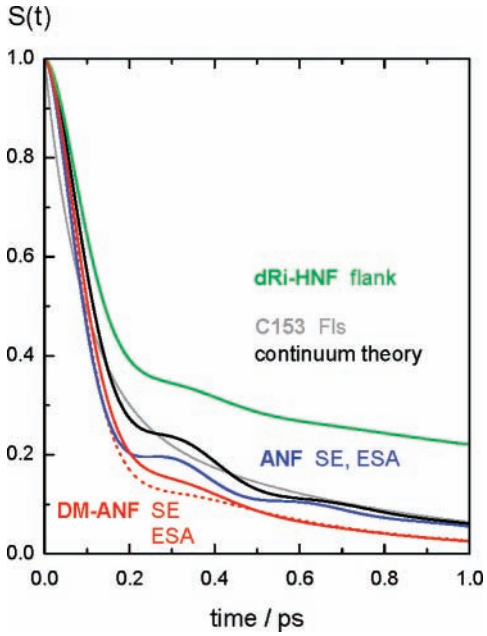

Figure 19. Comparison of relaxation functions $S(t)$ in acetonitrile. A solvent librational recurrence at ≈340 fs is observed with all nitrofluorene probes. Monitoring the stimulated emission (SE, solid lines) or excited-state absorption bands (ESA, dashed) gives the same results. The behavior of dRi-HNF (flank) is distorted by the onset of intersystem crossing. The relaxation function of C153 fluorescence[29] in acetonitrile is also shown (gray line).

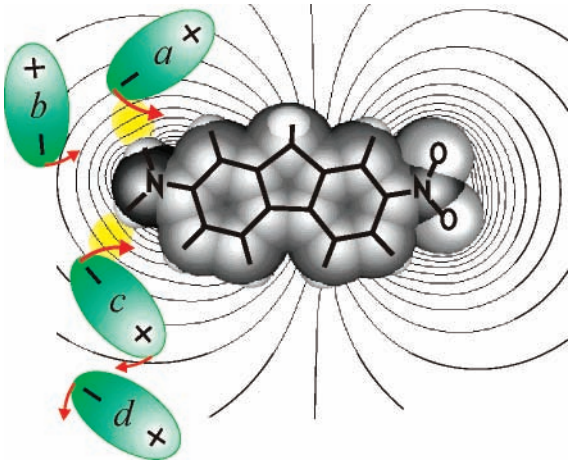

Figure 20. $S_1 \leftarrow S_0$ excitation of ANF perturbs solvent acetonitrile molecules $a-d$ by the electrostatic difference potential $\Delta\Phi$ (shown in steps of 10^{-3} esu/cm, black lines). Increased H bonding (yellow areas) causes additional torques on bonded acetonitriles *a* and *c*, kick-starting the libration of further solvent molecules *d*.

where H bonding is absent. On the other hand, for ANF/acn the extrapolated $\nu(0)$ falls 1730 cm^{-1} below the value from stationary spectroscopy. An initial portion of the reorganization energy is too fast to be detected. The defect could be related to changes of the H−N vibrational modes and associated H bonds in the S_1 state. The "kick-start" mechanism may also be operative when *N*-methyl-6-quinolone is solvated in methanol.[27] In this case, enhanced activity of the methanol C−O stretching mode was observed. (iii) The last reason for a change of solvent oscillations with molecular substitution at the probe may be that the cavity shape is affected. The effect may be illustrated by calculating $S(t)$ in acetonitrile from continuum theory, either in a spherical cavity as before or in a prolate cavity[95,96] with various numerical excentricities (see Supporting Information). Quantitative understanding of the observed solvation oscillations in terms of these possibilities requires more dedicated experiments. The main point here is that they can be observed at all, in quantifiably diverse detail, with the title compounds. Contrast this with the behavior of Coumarin 153 in acetonitrile. In this case we searched in vain for solvation oscillations, even though several excitation wavelengths, detection schemes, and experimental setups were used over several years. Their lack probably reflects a problem with the probe itself. The latter has a rich vibronic spectrum at low excess energy in S_1 even in the isolated molecule.[97] Interaction with the solvent libration at around 100 cm^{-1} could alter the dynamics of the first solvent shells substantially compared to the pure liquid. Thus, the slightly underdamped libration of pure acetonitrile may become critically damped, in which case it is not recognized. Rigidity of the probe is seen to be a key to finding the local FIR spectrum.

A practical conclusion from Figure 19 concerns the type of band which is monitored with substituted nitrofluorenes. The time-resolved shift of the ESA band is found to agree, within experimental errors, with that of the SE band. The latter is susceptible to systematic errors because of overlap with excited-state absorption, which has a different sign. The former does not appear to suffer to the same degree from the equivalent effect of stimulated emission; however, the ESA Stokes shift is only a third of the emission shift. That limitation can be overcome technically by increasing the spectrographic dispersion, in which case observation of the ESA band should be preferred in time-resolved solvation studies. Finally, recall that dRi-HNF is an imperfect probe of polar solvation because of the mixed $\pi\pi^*$/$n\pi^*$ character of the S_1 state and because incipient triplet absorption limits the observation window to ∼1 ps. Even though, the solvent oscillation in acetonitrile was detected as ±70 cm^{-1} frequency excursions of the stimulated emission band. The achieved sensitivity is sufficient to induce and observe vibrational coherence when the artificial nucleobase is incorporated in a DNA double helix.

5. Conclusion

Push−pull substituted fluorenes may be used as dynamic solvation probes in polynucleotides. Their femtosecond optical excitation at the $S_1 \leftarrow S_0$ absorption peak does not create intramolecular vibrational wavepackets. Nuclear coherence, which is induced in the environment, can therefore be detected as a frequency modulation of the evolving emission band. The concept was proved with 2-amino-7-nitrofluorene, 2-dimethylamino-7-nitrofluorene, 2-hydroxy-7-nitrofluorene, and its 2′-deoxyriboside in acetonitrile, which provides a solvent oscillation at 100 cm^{-1}. The latter was observed with all probes. Different strengths of the oscillation indicate that rotational friction depends on solute structure or that H bonding is involved in launching the coherence. Such dynamical use of H bonding should be sought when designing fluorescent probes for supramolecular structures. The S_1 state of 2-hydroxy-7-nitrofluorene has $\pi\pi^*$/$n\pi^*$ character, and intersystem crossing occurs on the 10 ps time scale. A prominent excited-state absorption band of nitrofluorenes at 430 nm can be used to monitor polar solvation.

Acknowledgment. This project was supported by the Deutsche Forschungsgemeinschaft. We thank Dennis Löwenich (Heinrich Heine University, Düsseldorf, Germany) for triplet spectra, John E. Bertie (University of Alberta, Edmonton, Canada) for dielectric dispersion data, and the Fond der Chemischen Industrie for general support.

Supporting Information Available: Fluorescence lifetimes of ANF and DMANF in several solvents, transient absorption spectra and spectral shifts, frontier orbitals of ANF and HNF, and dielectric dispersion of methanol and acetonitrile. This material is available free of charge via the Internet at http://pubs.acs.org.

References and Notes

(1) Benjamin, I. *Chem. Rev.* **2006**, *106*, 1212.
(2) Bagchi, B. *Chem. Rev.* **2005**, *105*, 3197.
(3) Pal, S. K.; Zewail, A. H. *Chem. Rev.* **2004**, *104*, 2099.
(4) Glasbeek, M.; Zhang, H. *Chem. Rev.* **2004**, *104*, 1929.
(5) Nandi, N.; Bhattacharyya, K.; Bagchi, B. *Chem. Rev.* **2000**, *100*, 2013.
(6) Jin, H.; Baker, G. A.; Arzhantsev, S.; Dong, J.; Maroncelli, M. *J. Phys. Chem. B* **2007**, *111*, 7291.
(7) Paul, A.; Samanta, A. *J. Phys. Chem. B* **2007**, *111*, 4724.
(8) Samanta, A. *J. Phys. Chem. B* **2006**, *110*, 13704.
(9) Shim, Y.; Choi, M. Y.; Kim, H. J. *J. Chem. Phys*, **2005**, *122*, 044511.
(10) Mandal, U.; Adhikari, A.; Dey, S.; Ghosh, S.; Mondal, S. K.; Bhattacharyya, K. *J. Phys. Chem. B* **2007**, *111*, 5896.
(11) Tamoto, Y.; Segawa, H.; Shirota, H. *Langmuir* **2005**, *21*, 3757.
(12) Sen, P.; Ghosh, S.; Mondal, S. K.; Sahu, K.; Roy, D.; Bhattacharyya, K.; Tominaga, K. *Chem.—Asian J.* **2006**, *1*−*2*,188.
(13) Kim, J.; Lu, W.; Qiu, W.; Wang, L.; Caffrey, M.; Zhong, D. *J. Phys. Chem. B* **2006**, *110*, 21994.
(14) Benderskii, A. V.; Eisenthal, K. B. *J. Phys. Chem. A* **2002**, *106*, 7482.
(15) Bürsing, H.; Kundu, S.; Vöhringer, P. *J. Phys. Chem. B* **2003**, *107*, 2404.
(16) Pal, S. K.; Peon, J.; Zewail, A. H. *Proc. Natl. Acad. Sci. U.S.A.* **2002**, *99*, 15297.
(17) Abbyad, P.; Shi, X.; Childs, W.; McAnaney, T. B.; Cohen, B. E.; Boxer, S. G. *J. Phys. Chem. B* **2007**, *111*, 7291.
(18) Golosov, A. A.; Karplus, M. *J. Phys. Chem. B* **2007**, *111*, 1482.
(19) Bandyopadhyay, S.; Chakraborty, S.; Bagchi, B. *J. Phys. Chem. B* **2006**, *110*, 20629.
(20) Zhang, L.; Kao, Y. -T.; Qiu, W.; Wang, L.; Zhong, D. *J. Phys. Chem. B* **2006**, *110*, 18097.
(21) Andreatta, D.; Sen, S.; Lustres, J. L. P.; Kovalenko, S. A.; Ernsting, N. P.; Murphy, C. J.; Coleman, R. S.; Berg, M. A. *J. Am. Chem. Soc.* **2006**, *128*, 6885.
(22) Pal, S.; Maiti, P. K.; Bagchi, B.; Hynes, J. T. *J. Phys. Chem. B* **2006**, *110*, 26396.
(23) Maroncelli, M.; Fleming, G. R. *J. Chem. Phys.* **1987**, *86*, 6221.
(24) Beveridge, D. L.; Schnuelle, G. W. *J. Phys. Chem.* **1975**, *79*, 2562.
(25) (a) Hsu, C. P.; Song, X.; Marcus, R. A. *J. Phys. Chem. B* **1997**, *101*, 2546. (b) Hsu, C. P.; Georgievskii, Y.; Marcus, R. A. *J. Phys. Chem. A* **1998**, *102*, 2658.
(26) Song, X.; Chandler, D. *J. Chem. Phys.* **1998**, *108*, 2594.
(27) Lustres, J. L. P.; Kovalenko, S. A.; Mosquera, M.; Senyushkina, T.; Flasche, W.; Ernsting, N. P. *Angew. Chem., Int. Ed.* **2005**, *44*, 5635.
(28) Ruthmann, J.; Kovalenko, S. A.; Ernsting, N. P.; Ouw, D. *J. Chem. Phys*. **1998**, *109*, 5466.
(29) Horng, M. L.; Gardecki, J. A.; Papazyan, A.; Maroncelli, M. *J. Phys. Chem*. **1995**, *99*, 17311.
(30) Brauns, E. B.; Madaras, M. L.; Coleman, R. S.; Murphy, C. J.; Berg, M. A. *J. Am. Chem. Soc*. **1999**, *121*, 11644.
(31) Coleman, R. S.; Madaras, M. L. *J. Org. Chem*. **1998**, *63*, 5700.
(32) Fiebig, T.; Wan, C.; Zewail, A. H. *ChemPhysChem* **2002**, *3*, 781.
(33) Wan, C.; Xia, T.; Becker, H.-C.; Zewail, A. H. *Chem. Phys. Lett.* **2005**, *412*, 158.
(34) O'Neill, M. A.; Barton, J. K. *J. Am. Chem. Soc*. **2002**, *124*, 13053.
(35) Nordlund, T. M.; Andersson, S.; Nilsson, L.; Rigler, R.; Gräslund, A.; McLaughlin, L. W. *Biochemistry* **1989**, *28*, 9095.
(36) Pal, S. K.; Zhao, L.; Xia, T.; Zewail, A. H.; *Proc. Natl. Acad. Sci. U.S.A.* **2003**, *100*, 13746.
(37) van der Zwan, G.; Hynes, J. T. *J. Phys.Chem*. **1985**, *89*, 4181.
(38) Ladanyi, B. M.; Stratt, R. M. *J. Phys. Chem.* **1995**, *99*, 2502.
(39) Wan, Y.; Stratt, R. M. *J. Chem. Phys*. **1994**, *100*, 5123.
(40) Rosenthal, S. J.; Xie, X.; Du, M.; Fleming, G. R. *J. Chem. Phys*. **1991**, *95*, 4715.
(41) Dobryakov, A. L.; Ernsting, N. P.; In *Analysis and Control of Ultrafast Photoinduced Reactions*; Kühn, O., Wöste, L., Eds.; Springer Series in Chemical Physics, Vol. 87; Springer: Heidelberg, Germany, 2007; p 689.
(42) (a) Nibbering, E. T. J.; Wiersma; D. A.; Duppen, K. *Chem. Phys.* **1994**, *183*, 167. (b) de Boeij, W. P.; Pshenichnikov, M. S.; Wiersma, D. A. *Chem. Phys. Lett.* **1995**, *247*, 264.
(43) (a) Cho, M.; Fleming, G. R. *J. Chem. Phys*. **1993**, *98*, 2848. (b) Joo, T.; Jia, Y.; Fleming, G. R. *J. Chem. Phys*. **1995**, *102*, 4063. (c) Larsen, D. S.; Ohta, K.; Xu, Q.-H.; Cyrier, M.; Fleming, G. R. *J. Chem. Phys*. **2001**, *114*, 8008. (d) Ohta, K.; Larsen, D. S.; Yang, M.; Fleming, G. R. *J. Chem. Phys.* **2001**, *114*, 8020.
(44) Maroncelli, M. *J. Chem. Phys.* **1991**, *94*, 2084.
(45) Chandra, A.; Bagchi, B. *J. Chem. Phys*, **1991**, *94*, 3177.
(46) Ingrosso, F.; Ladanyi, B. M.; Mennucci, B.; Elola, M. S.; Tomasi, J. *J. Phys. Chem B* **2005**, *109*, 3553.
(47) Jeannin, C.; Portella-Oberli, M. T.; Jimenez, S.; Vigliotti, F.; Lang, B.; Chergui, M. *Chem. Phys. Lett.* **2000**, *316*, 51.
(48) Gühr, M.; Schwentner, N. *Phys. Chem. Chem. Phys.* **2005**, *7*,760.
(49) Barbara, P. F.; Jarzeba, W. *Adv. Photochem.* **1990**, *15*, 1.
(50) Jimenez, R.; Fleming, G. R.; Kumar, P. V.; Maroncelli, M. *Nature* **1994**, *369*, 471.
(51) Jarzeba, W.; Walker, G. C.; Johnson, A. E.; Kahlow, M. A.; Barbara, P. F. *J. Phys. Chem*. **1988**, *92*, 7039.
(52) Maroncelli, M.; Fleming, G. R. *J. Chem. Phys.* **1988**, *89*, 5044.
(53) Silva, C.; Walhout, P. K.; Yokoyama, K.; Barbara, P. *Phys. Rev. Lett.* **1998**, *80*, 1086.
(54) Zolotov, B.; Gan, A.; Fainberg, B. D.; Huppert, D. *Chem. Phys. Lett.* **1997**, *265*, 418.
(55) Ohba, T.; Ikawa, S. *Mol. Phys.* **1991**, *73*, 985.
(56) Saroja, G.; Pingzhu, Z.; Ernsting, N. P.; Liebscher, J. *J. Org. Chem.* **2004**, *69*, 987.
(57) Rieveschl, G., Jr.; Earl Ray, F. *Chem. Rev.* **1938**, *23*, 287.
(58) Jones, W. D., Jr.; Albrecht, W. L.; Palopoli, F. P. *J. Org. Chem.* **1977**, *42*, 4144.
(59) Bryant, H.; Sawicki, E. *J. Org. Chem.* **1956**, *21*, 1322.
(60) Dahlgard, M. *J. Org. Chem.* **1960**, *25*, 469.
(61) Sklenar, H.; Wüstner, D.; Rohs, R. *J. Comput. Chem.* **2006**, *27*, 309.
(62) Cornell, W. D.; Cieplak, P.; Bayly, C. I.; Gould, I. R.; Merz, K. M., Jr.; Ferguson, D. M.; Spellmeyer, D. C.; Fox, T.; Caldwell, J. W.; Kollman, P. A. *J. Am. Chem. Soc*. **1995**, *117*, 5179.
(63) Lavery, R.; Sklenar, H.; Zakrzewska, K.; Pullman, B. *J. Biomol. Struct. Dyn.* **1986**, *3*, 989.
(64) Rohs, R.; Sklenar, H.; Shakked, Z. *Structure* **2005**, *13*, 1499.
(65) Rohs, R.; Bloch, I.; Sklenar, H.; Shakked, Z. *Nucleic Acids Res.* **2005**, *33*, 7048.
(66) Lavery, R.; Zakrzewska, K.; Sklenar, H. *Comput. Phys. Commun.* **1995**, *91*, 135.
(67) Frisch, M. J.; Trucks, G. W.; Schlegel, H. B.; Scuseria, G. E.; Robb, M. A.; Cheeseman, J. R.; Zakrzewski, V. G.; Montgomery, J. A., Jr.; Stratmann, R. E.; Burant, J. C.; Dapprich, S.; Millam, J. M.; Daniels, A. D.; Kudin, K. N.; Strain, M. C.; Farkas, O.; Tomasi, J.; Barone, V.; Cossi, M.; Cammi, R.; Mennucci, B.; Pomelli, C.; Adamo, C.; Clifford, S.; Ochterski, J.; Petersson, G. A.; Ayala, P. Y.; Cui, Q.; Morokuma, K.; Malick, D. K.; Rabuck, A. D.; Raghavachari, K.; Foresman, J. B.; Cioslowski, J.; Ortiz, J. V.; Stefanov, B. B.; Liu, G.; Liashenko, A.; Piskorz, P.; Komaromi, I.; Gomperts, R.; Martin, R. L.; Fox, D. J.; Keith, T.; Al-Laham, M. A.; Peng, C. Y.; Nanayakkara, A.; Gonzalez, C.; Challacombe, M.; Gill, P. M. W.; Johnson, B. G.; Chen, W.; Wong, M. W.; Andres, J. L.; Head-Gordon, M.; Replogle, E. S.; Pople, J. A. *Gaussian 98*, revision A.3; Gaussian, Inc.: Pittsburgh, PA, 1998.
(68) Karunakaran, V.; Senyushkina, T.; Saroja, G.; Liebscher, J.; Ernsting, N. P. *J. Phys. Chem. A* **2007**, *111*, 10944.
(69) Laikov, D. N. *Chem. Phys. Lett.* **1997**, *281*, 151.
(70) Perdew, J. P.; Burke, K.; Ernzerhof, M. *Phys. Rev. Lett.* **1996**, *77*, 3865.
(71) Granovsky, A. A. *PC GAMESS*, version 7.1; Moscow State University: Moscow, Russia, 2007.
(72) Schuchardt, K. L.; Didier, B. T.; Elsethagen, T.; Sun, L.; Gurumoorthi, V.; Chase, J.; Li, J.; Windus, T. L. *J. Chem. Inf. Model.* **2007**, *47*, 1045.
(73) Kovalenko, S. A.; Dobryakov, A. L.; Ruthmann, J.; Ernsting, N. P. *Phys. Rev. A* **1999**, 59, 2369.
(74) (a) Catalán, J.; López, V.; Pérez, P.; Villamil, R. M-.; Rodriguez, J.-G. *Liebigs Ann*. **1995**, 241. (b) Catalán, J.; López, V.; Pérez, P. *Liebigs Ann*. **1995**, 793.
(75) Lippert, E. *Z. Elektrochem*. **1957**, *61*, 962.
(76) Mukamel, S. *Principles of Nonlinear Optical Spectroscopy*; Oxford University: New York, 1995.
(77) Dobryakov, A. L.; Kovalenko, S. A.; Ernsting, N. P. *J. Chem. Phys.* **2003**, *119*, 988.
(78) Dobryakov, A. L.; Kovalenko, S. A.; Ernsting, N. P. *J. Chem. Phys.* **2005**, *123*, 44502.
(79) Ernsting, N. P.; Kovalenko, S. A.; Senyushkina, T.; Saam, J.; Fartzdinov, V. *J. Phys. Chem. A* **2001**, *105*, *3443*.
(80) See Supporting Information.
(81) Sklenar, H.; Rohs, R. *J. Biomol. Struct. Dyn.* **2003**, *20*, 835.
(82) In Figure 3, only the part with $\nu > 0$ represents stable modes and may be identified with the FIR (a) or the solvation spectrum (b). The

contribution of unstable modes to the solvation spectrum is relatively small (compared to the FIR spectrum here or to that of common liquids[38]). This is why instantaneous normal mode theory may be applied, in this case, up to a few hundred femtoseconds for a qualitative estimate of the oscillations of $\nu(t)$.

(83) Birks, J. B. *Photophysics of Aromatic Molecules*; Wiley-Interscience, New York, 1970.

(84) A modified relation is needed if solvation proceeds during most of the S_1 lifetime.

(85) Siano, D. B.; Metzler, D. E. *J. Chem. Phys*. **1969**, *51*, 1856.

(86) Risken, H.; *The Fokker-Planck Equation*, 2nd ed.; Springer-Verlag, Berlin, 1989; Chapter 10.2. In the present case, we have $\nu(0) - \nu(\infty) = 6090\ \mathrm{cm}^{-1}$, $\Delta(0) - \Delta(\infty) = 1230\ \mathrm{cm}^{-1}$, and $\gamma(0) - \gamma(\infty) = 0.0146$.

(87) Mondal, J. A.; Sarkar, M.; Samanta, A.; Ghosh, H. N.; Palit, D. K. *J. Phys. Chem. A* **2007**, *111*, 6122.

(88) Other schemes are possible, for example, $S_1 \xrightarrow{\Phi \cdot k1} X \xrightarrow{k2} T_1$ together with $S_1 \xrightarrow{(1-\Phi)\cdot k1} T$, but from the X-associated spectrum it follows that $\Phi \geq 0.8$.

(89) In principle, the solvent Raman contribution can be determined separately and subtracted. In practice, the error of the procedure is large since the time-resolved fluorescence signal from the chromophore is smaller by several orders of magnitude.

(90) Kovalenko, S. A.; Ruthmann, J.; Ernsting, N. P. *Chem. Phys. Lett.* **1997**, *271*, 40.

(91) Marcus, Y.; Kamlet, M. J.; Taft, R. W. *J. Phys. Chem.* **1988**, *92*, 3613.

(92) Kamlet, M. J.; Abboud, J. L. M.; Abraham, M. H.; Taft, R. W. *J. Org. Chem.* **1983**, *48*, 2877.

(93) Pines, E.; Pines, D.; Ma, Y.-Z.; Fleming, G. R. *ChemPhysChem* **2004**, *5*, 1315.

(94) Fee, R. S.; Maroncelli, M. *Chem. Phys.* **1994**, *183*, 235.

(95) Hsu, C.-P.; Song, X.; Marcus, R. A. *J. Phys. Chem. B* **1997**, *101*, 2546.

(96) Böttcher, C. J. F. *Theory of Electric Polarization*, 2nd ed.; Elsevier Science Publishers: Amsterdam, The Netherlands, 1993; Vol. I, pp 137, 80.

(97) Mühlpfordt, A.; Schanz, R.; Ernsting, N. P.; Varztdinov, V.; Grimme, S. *Phys. Chem. Chem. Phys.* **1999**, *1*, 3209.